Rare Met. (2020) 39(10):1165–1173
https://doi.org/10.1007/s12598-019-01298-z

RARE METALS
www.editorialmanager.com/rmet

First-principles calculation of $Au_n@(ZnS)_{42}$ (n = 6–16) hetero-nanostructure system

Han-Yue Zhao, Qing Liu, Xiao-Xu Wang, Jin-Rong Huo, Lu Li, Ping Qian, Yan-Jing Su*

Received: 13 November 2018 / Revised: 24 January 2019 / Accepted: 20 May 2019 / Published online: 26 August 2019

Abstract The structure stability and electronic and optical properties of a series of Au@ZnS core–shell nanocomposites with different sizes were investigated theoretically by first-principle calculation based on density functional theory (DFT). A series of $Au_n@(ZnS)_{42}$ structures with different n values from 6 to 16 were optimized and obtained. Based on the core–shell interaction energy and second-order difference of total energy of these structures, it is found that $Au_{13}@(ZnS)_{42}$ turns out to be the most stable structure. Based on the model of $Au_{13}@(ZnS)_{42}$, the density of state and charge density difference were studied and provided a deeper understanding of the electronic structures of Au@ZnS. On the other hand, absorption coefficient and dielectric function were investigated to study the optical properties. It is found that an optical absorption peak appears in visible-light region, indicating that the photo-catalytic can be improved prominently due to the optical redshift to visible-light region when forming core–shell structure from ZnS bulk. And the redshift phenomenon accords well with experiment. Furthermore, the electronic structure further confirms the existence of redshift of optical absorption spectrum.

Keywords Core–shell structure; Density functional theory (DFT); Electronic structure; Optical properties; Redshift phenomenon

1 Introduction

Core–shell nanoparticles have received tremendous attentions in materials science and engineering due to the wide application in different areas such as catalysis [1–3], electronics [4, 5], biomedical [6, 7] and enhancing photoluminescence [8] with the advantages of avoiding the inner core exposure to solvent and maximizing the interaction between the core and shell. By controlling chemical constitution, size and morphology, the adjustable properties of core–shell structure can be utilized to a large range of different fields. In particular, core–shell nanoclusters comprised of noble metal core and semiconductor shell as building blocks have emerged as a quiet promising system in recent years [9, 10] because of their peculiar structures and remarkable physicochemical properties compared with individual component nanomaterial.

Among all kinds of semiconductors, ZnS as one of the most popular photo-catalysts plays an important role in photonics that have been extensively utilized in emission devices, cathodoluminescence, light-emitting diodes and sensors [11–13]. However, the visible-light photocatalyst application has been restricted by the low visible-light absorption of ZnS. To overcome this problem, one of the most promising way is to involve noble metals with

Han-Yue Zhao and Qing Liu have contributed equally to this work.

H.-Y. Zhao, Q. Liu, X.-X. Wang, J.-R. Huo, L. Li, P. Qian, Y.-J. Su*
Beijing Advanced Innovation Center for Materials Genome Engineering, University of Science and Technology Beijing, Beijing 100083, China
e-mail: yjsu@ustb.edu.cn

H.-Y. Zhao, Q. Liu, X.-X. Wang, J.-R. Huo, L. Li, P. Qian
Department of Physics, University of Science and Technology Beijing, Beijing 100083, China

Y.-J. Su
Corrosion and Protection Center, Key Laboratory for Environmental Fracture (MOE), University of Science and Technology Beijing, Beijing 100083, China

complementary properties to ZnS structure. For instance, it has been reported that the introduction of Au clusters into ZnS structure benefits the photo-catalytic activity by extending the optical absorption edge to the visible-light region [14]. In the past decade, the Au–ZnS nanocomposites with different morphologies have been discussed extensively.

For example, Chen et al. [15] have prepared core-satellite ZnS–Au nano-assemblies, in which each of the ZnS nanosphere was surrounded by a few Au nanoparticles. It exhibited high photo-catalytic efficiency and thus was applied for degradation of cationic dye (TH) under ultraviolet–visible (UV) light. Zhang et al. [16] have synthesized Au nanoparticles loaded on ZnS nanostructures. They found that Au nanoparticles obviously enhanced photo-catalytic hydrogen production rate of ZnS structure. Geng et al. [17] have synthesized Au–ZnS hybrid nanostructure. The formation mechanism and optical properties of the nanocomposites with different Au doping concentrations were also discussed. Sagheer and Madkour [18] found that a significant increase in the photo-catalytic activity takes place upon the loading of Au nanoparticles on ZnS. And the optoelectronic properties of the nanoparticles in terms of band structure were determined.

However, for the above Au–ZnS nanocomposites, Au nanoparticles exposed to the surrounding environment are likely to suffer from corrosion and thus reduce catalytic activity. Core–shell composite can resist corrosion by insulating the metallic core from its surroundings environment.

For example, Mrinmoy et al. [14] have proposed a simple, novel and quick preparation of Au@ZnS core–shell nanostructure. They have investigated the effect of Au core concentration on electrical properties and optical behavior. The visible photo-catalytic activity was observed to get improved with the increase in concentration of Au core in Au@ZnS nanostructure. In summary, when putting Au cluster as the inner core of ZnS outer shell, Au@ZnS core–shell nanoparticles will exhibit excellent photoelectron property and enhanced catalytic performance compared with individual component material.

Nevertheless, there are not many researches about Au@ZnS nanocomposite experimentally and theoretically, and the synthesis of Au@ZnS nanoparticles is still a challenge, although there have been a few successful preparations. Especially, as we can see, most works pay more attention to the experimental process and description of the phenomenon. The theoretical study about the physical mechanism and the explanation of experiment results is still scarce, which has become a major roadblock for the investigation of core–shell structure. In this work, the structural stability and functional properties of a series of $Au_n@(ZnS)_{42}$ (n = 6–16) nanocomposites were investigated by density functional theory (DFT) which include finding the most stable nanostructure and studying their electronic and optical properties.

2 Computational methods

In this study, first-principles calculation based on DFT was performed to investigate Ag@ZnS core–shell nanostructure, as implemented in Vienna ab initio simulation package (VASP). The generalized gradient approximation (GGA) methods as described by Perdew, Burke and Ernzerhof (PBE) [19] was chosen to describe the exchange correlation function. A plane wave basis was set with a cutoff energy of 480 eV, and only the gamma point sampling of the Brillouin zone was adopted for the core–shell nanostructure calculations. A cubic box with side length of 2 nm was used to contain the particle in all directions to reduce the interactions between periodic images. All atoms in model systems were fully relaxed to obtain optimized structures with the convergence criteria for energy and maximum force of 1.0×10^{-5} eV and 0.05 eV·nm^{-1}, respectively. The structural relaxation terminated until the criteria were satisfied. The electronic and optical properties were calculated based on the optimized Ag@ZnS nanostructures.

3 Results and discussion

3.1 Structural properties of $Au_n@(ZnS)_{42}$ (n = 6–16) hetero-nanostructure

3.1.1 Structural properties of $Au_n@(ZnS)_{42}$ (n = 6–16)

The multiplicity and indeterminacy of core–shell heterostructure involve huge difficulties in the theoretical investigation of core–shell structure. With the lack of a proper model and the increasing number of atoms, the optimization of obtaining a stable structure in DFT calculation usually fails. Here, a series structures of $Au_n@(ZnS)_{42}$ with different numbers of Au atoms (n) were built. Inspired by the work on Au@ZnO [20] and TM@ZnO (TM = Fe, Co, Ni) [21], Au@ZnS structure was constructed since ZnO and ZnS share the similar wurtzite structure in bulk materials. Then, the structure was optimized by using conjugate gradient algorithm until the criteria of the convergence tolerance of energy and maximum force were reached. The obtained converged structure of $Au_n@(ZnS)_{42}$ for n from 6 to 16 is shown in Fig. 1. It can be seen that for these stable core–shell structure, the shapes of the outer shell remain almost unchanged with just slight differences.

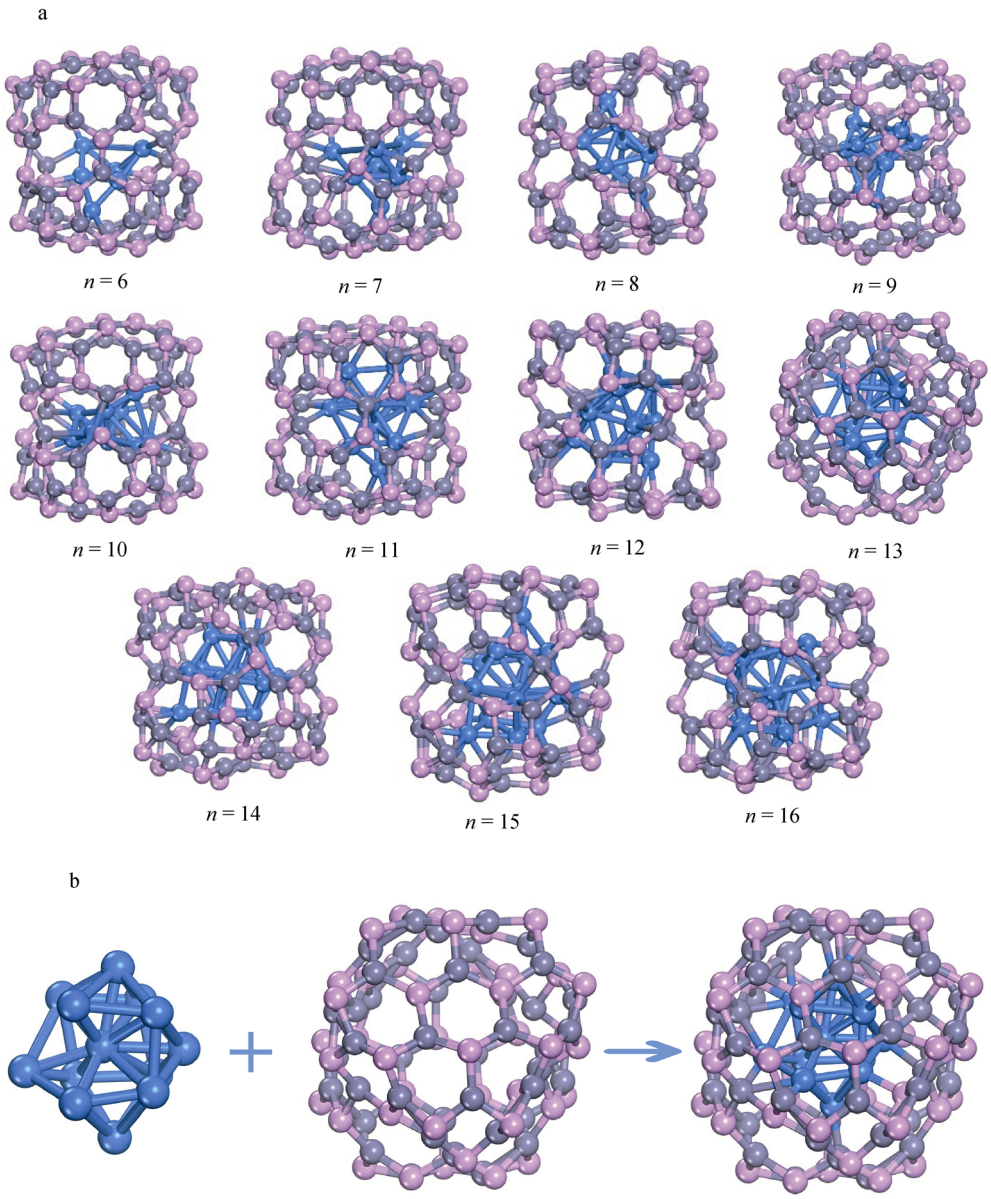

Fig. 1 Converged geometries of **a** $Au_n@(ZnS)_{42}$ core–shell nanostructure for n from 6 to 16 and **b** $Au_{13}@(ZnS)_{42}$ core–shell nanostructure, where blue, gray and pink balls refer to Au, Zn and S atoms, respectively

To investigate the relative stability among these structures with different sizes of inner core, as shown in Fig. 2, the core–shell interaction energy (E_{cs}) and the second-order difference of total energy ($\Delta_2 E$) are displayed, respectively. The core–shell interaction energy (E_{cs}) is defined as:

$$E_{cs} = (E_n - E_{core} - E_{shell})/N \quad (1)$$

where $N = n + 42$ is the total atom number of $Au_n@(ZnS)_{42}$ and E_n, E_{core} and E_{shell} are the total energy of $Au_n@(ZnS)_{42}$, Au_n inner core and $(ZnS)_{42}$ outer shell, respectively. The second-order differences of total energies ($\Delta_2 E$) are calculated as:

$$\Delta_2 E_n = E_{n-1} + E_{n+1} - 2E_n \quad (2)$$

where E_n is the total energy and n is the number of Au atoms.

It can be noted that the second-order differences of total energies and core–shell interaction energy are sensitive to the structure stability of nanoparticles. As shown in Fig. 2, the core–shell interaction energy reaches a minimum and $\Delta_2 E$ is maximal at $Au_{13}@(ZnS)_{42}$, indicating that $Au_{13}@(ZnS)_{42}$ is the most stable structure. It is reported that Au13 cluster is particularly stable which is well-known "magic numbers" [22]. That is also why $Au_{13}@(ZnS)_{42}$ core–shell composite with 13-Au acting as the inner core exhibits enhanced stability compared with other Au_n clusters.

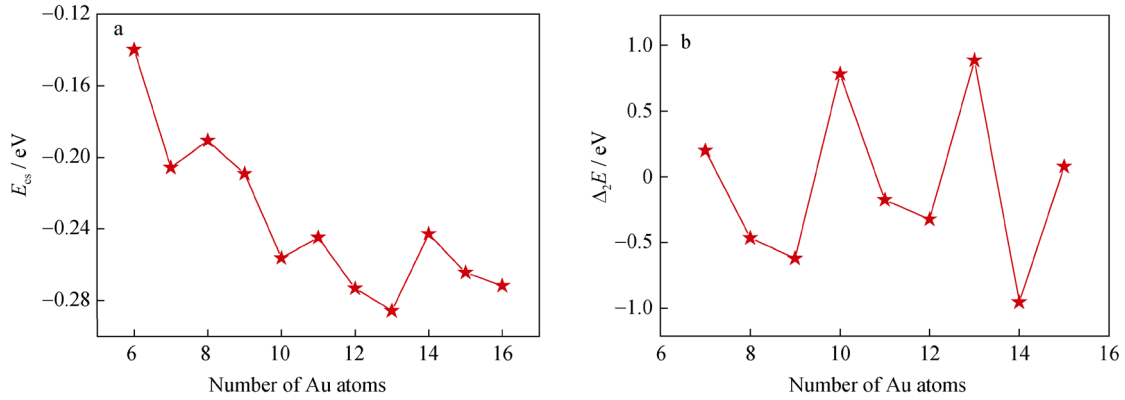

Fig. 2 **a** Core–shell interaction energy (E_{cs}) and **b** second-order difference of total energy (Δ_2E) of $Au_n@(ZnS)_{42}$(n = 6–16) nanostructures, where minimum E_{cs} and maximal Δ_2E at n = 13 indicate that $Au_{13}@(ZnS)_{42}$ is the most stable structure

The calculated average bond lengths are also demonstrated in Table 1 and compared with bulk ZnS and bulk Au. The results show that the bond lengths of Zn–Zn, Zn–S and Au–Au all decrease compared with that of bulk materials, which means that the outer shell and inner core tend to contract and become denser to form a stable united structure.

3.1.2 Structural properties of Au cluster

In addition, structural properties of Au cluster in shell from the isolated one are also discussed. In Fig. 3, the optimized structures of Au13 isolated cluster and Au13 core separated from outer shell are shown, respectively. As can be clearly seen that when putting Au13 cluster in ZnS outer shell, optimized Au13 core shows some deformation compared with the isolated cluster, which is likely attributed to strong interfacial electronic interaction between Au inner core and ZnS outer shell.

3.1.3 Interface properties of $Au_{13}@(ZnS)_{42}$

For core–shell nanostructure, it is of great importance to investigate the interface between Au cluster and ZnS shell, which is closely associated with functions and properties of nanostructure. Au–S and Au–Zn nearest distance at

Table 1 Calculated average bond length of Zn–S, Zn–Zn and Au–Au for bulk ZnS, bulk Au and $Au_{13}@(ZnS)_{42}$ core–shell nanostructure, respectively, and experimental bond lengths presented (in brackets) for comparison (nm)

Structure	Bulk-ZnS/bulk-Au	$Au_{13}@(ZnS)_{42}$
Zn–S distance	0.2359 (0.235 [23])	0.2307
Zn–Zn distance	0.3860	0.3445
Au–Au distance	0.2884 (2.88 [24])	0.2848

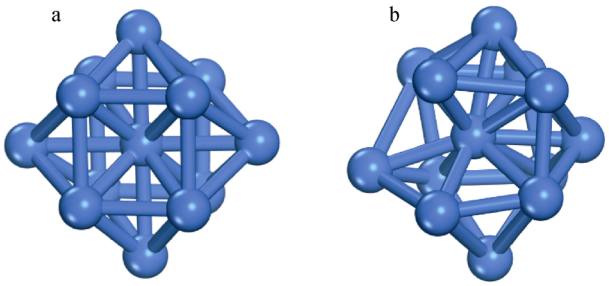

Fig. 3 Optimized structures of **a** Au13 isolated cluster and **b** Au13 core separated from ZnS outer shell

interface for $Au_{13}@(ZnS)_{42}$ are shown in Table 2. And charge transfer between core and shell for per Au is also presented. From Table 2, it can be concluded that, except for a few cases, the smaller the Au–S distance or Au–Zn distance is, the more the charge transfer occurs between Au core and ZnS shell. For example, for $Au_{13}@(ZnS)_{42}$ nanostructure, Au2 atom has more charge transfer of 0.159 than the average value of 0.117, with corresponding smaller Au–S distance of 0.2676 nm. Another example, Au11 atom has more charge transfer of 0.190, which is corresponding to smaller Au–Zn distance of 0.2611 nm.

In addition, from core–shell nanostructure in Fig. 1, it can be seen that some S atoms move toward the surface, and part of Zn atoms toward internal, which will lead to the atom recombination on the shell. Therefore, Au@ZnS core–shell structure can be approximately regarded as one side for Zn termination and the other side for O termination at the interface of core–shell, which is similar to other work about Ag@ZnO nanostructure [25]. On the other hand, some Au, Zn and S atoms blend together at the interface, indicating that the inter-attraction between Au cluster and ZnS shell further enhances the relativistic effect (RE) and promotes bonds formation at the interface.

Table 2 Au–S and Au–Zn nearest distance and charge transfer for $Au_{13}@(ZnS)_{42}$

Clusters	Au–S distance/nm	Au–Zn distance/nm	Charge transfer/e
Au1	0.3679	0.2676	0.251
Au2	0.2676	0.2790	0.159
Au3	0.2426	0.3482	0.053
Au4	0.2394	0.3526	0.047
Au5	0.3819	0.2602	0.296
Au6	–	–	0.211
Au7	0.2439	0.2936	0.032
Au8	0.2451	0.2791	0.100
Au9	0.2486	0.2610	0.059
Au10	0.2436	0.2856	0.064
Au11	0.3615	0.2611	0.190
Au12	0.2478	0.2797	0.032
Au13	0.2476	0.2959	0.026
Average	0.2781	0.2880	0.117

3.2 Electronic structure properties of $Au_n@(ZnS)_{42}$ (n = 6–16) hetero-nanostructure

3.2.1 Electronic structure properties of $Au_{13}@(ZnS)_{42}$ (n = 6–16) nanostructure

In order to get deep insights into the electronic structure, the spin-polarized electronic densities of states (DOS) of the stable structure $Au_{13}@(ZnS)_{42}$ and bulk-ZnS structures were all calculated for comparison. Figure 4 shows the total and partial DOS of $Au_{13}@(ZnS)_{42}$ composite and ZnS bulk structures. The total DOS (TDOS) near Fermi level is displayed as the inset. It is easy to see that there is a great difference in DOS curves between $Au_{13}@(ZnS)_{42}$ and ZnS bulk structure. From the total DOS curve of $Au_{13}@(ZnS)_{42}$, it can be found that it is mainly composed of two components. One of them locates at low-energy level region, and S-s, S-p, Zn-d and Au-d orbitals have a large contribution to the DOS. The other one is near the Fermi level, which is mainly originated from S-s, S-p and

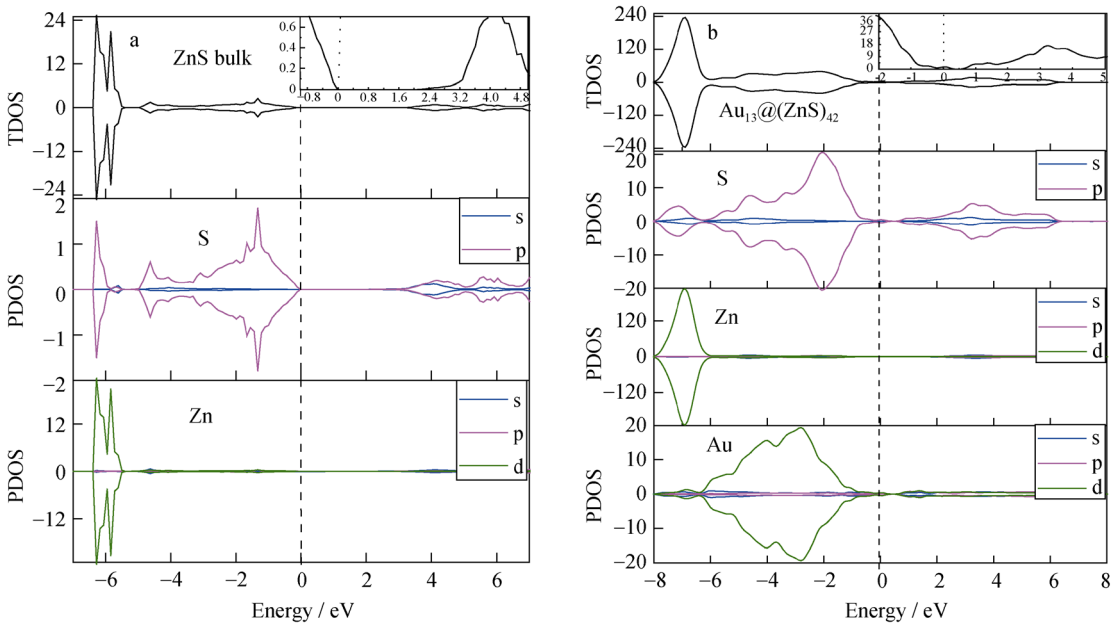

Fig. 4 Total and partial DOS of **a** ZnS bulk structure and **b** $Au_{13}@(ZnS)_{42}$ core–shell nanostructure, where total DOS (TDOS) near Fermi level is displayed as inset, dotted lines refer to Fermi level with unit of electrons·eV^{-1}

Zn-s, Au-d orbitals. For bulk ZnS structure, the DOS located at low-energy level mainly comes from the S-s, S-p and Zn-d orbitals, and the energy region near the Fermi level is mainly built up from the S-p state.

As can be seen from the inset of TDOS of wurtzite ZnS bulk structure, band gap between valence band and conduction band is about 2.3 eV, which is similar to other calculation works, such as 2.232 eV [26]. From the inset of $Au_{13}@(ZnS)_{42}$ TDOS, it can be noted that there also exists energy gap at Fermi level for the $Au_{13}@(ZnS)_{42}$ structure, indicating a semiconductor behavior for the core–shell configurations. But, the energy gap between the valence band maximum (VBM) and the conduction band minimum (CBM) of the $Au_{13}@(ZnS)_{42}$ is very small, which may be attributed to the occurrence of gap states near the Fermi level. The partial density of state (PDOS) for $Au_{13}@(ZnS)_{42}$ shows that gap states mainly result from S-p, Au-d orbitals, implying a lot of electrons interactions between Au-d and the S-p orbitals near the Fermi level. In other words, when doping Au cluster as inner core of ZnS outer shell, the core–shell interaction results in the occurrence of the hybridization between Au atom and its neighboring S atom. Besides, Au-d and S-p hybridization may partly help to explain why the nanostructure stability enhances when Au-cluster serving as the inner core in ZnS outer shell.

The above conclusion can be confirmed by the calculated charge density difference, as presented in Fig. 5a and b. It can be clearly seen that a large number of charges are lost from the Au atoms of inner core, and the interface region between inner core and out shell is occupied by a higher bonding charge. That is to say, there exists the obvious electron transfer between the Au atom and neighbor S atom. The above indicates strong electrons interaction between inner core and outer shell region, which leads to the formation of Au–S bonds.

To obtain a better understanding for electronic structure properties at interface, the 2D charge density difference of $Au_{13}@(ZnS)_{42}$ nanocluster is shown in Fig. 6 and charge

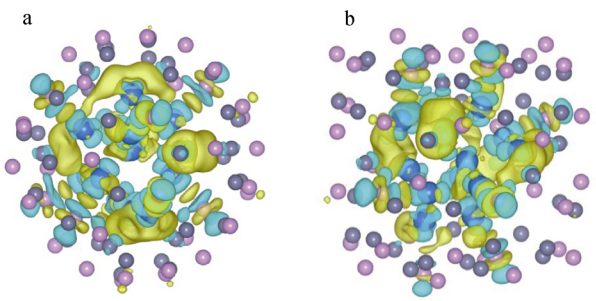

Fig. 5 Plot of charge density difference for $Au_{13}@(ZnS)_{42}$ core–shell nanocluster: **a** top view and **b** side view, where loss and enrichment of electrons are displayed in light blue and yellow, respectively, and isosurface value used is 20.24 e·nm^{-3}

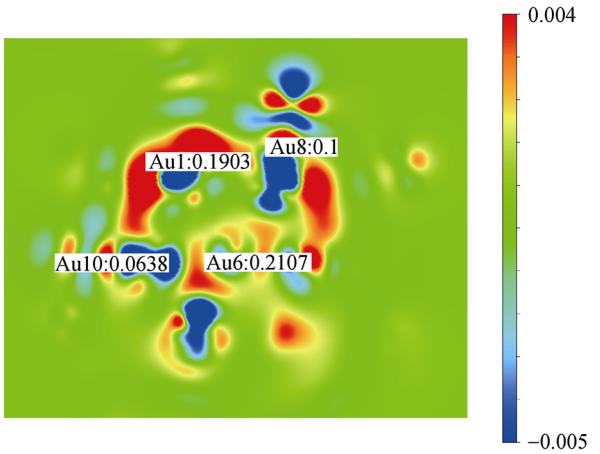

Fig. 6 Plot of 2D charge density difference for $Au_{13}@(ZnO)_{42}$ with charge transfer data of typical atom marked out (unit: e)

transfer data of the typical atom have also been marked out. It can be further confirmed that there are a lot of electrons accumulated at interface and lots of electrons transfer from Au atoms and ZnS shell.

As we all know, because the Fermi energy level of Au is higher than that of ZnS structure, the electrons transfer from valence band of Au cluster to ZnS conduction band will occur. Therefore, these new occupied states near the Fermi energy level supply a bridge for electrons excitation. And the electron excitation may lead to a significant redshift of the absorption spectrum, that is, a new optical absorption in the visible-light region. The redshift phenomenon is also found in other core–shell nanoclusters, theoretically and experimentally [20, 27–29]. The optical property of Au@ZnS nanocluster is very complex. Therefore, in the next section, the optical properties of the $Au_{13}@(ZnS)_{42}$ core–shell nanostructure will be discussed in detail.

3.2.2 *Electronic structure properties of Au cluster*

In order to understand the difference of electronic structure properties of Au cluster in shell with the isolated one, the total density of state (TDOS) and partial density of state (PDOS) of Au13 isolated cluster and Au13 inner core are displayed in Fig. 7. As can be seen that, when putting Au13 cluster in the ZnS outer shell, the integrity of DOS of Au13 inner core becomes weak, which indicates that some electrons are lost and transfer from Au cluster to ZnS outer shell. The conclusion is consistent with the above discussion in electronic structure properties of $Au_{13}@(ZnS)_{42}$ core–shell nanostructure.

In addition, it can also be seen that the DOS curves of Au13 inner core become smoother and some peaks disappear compared with isolated cluster, which is mainly due to strong electrons interaction between Au core and ZnS outer

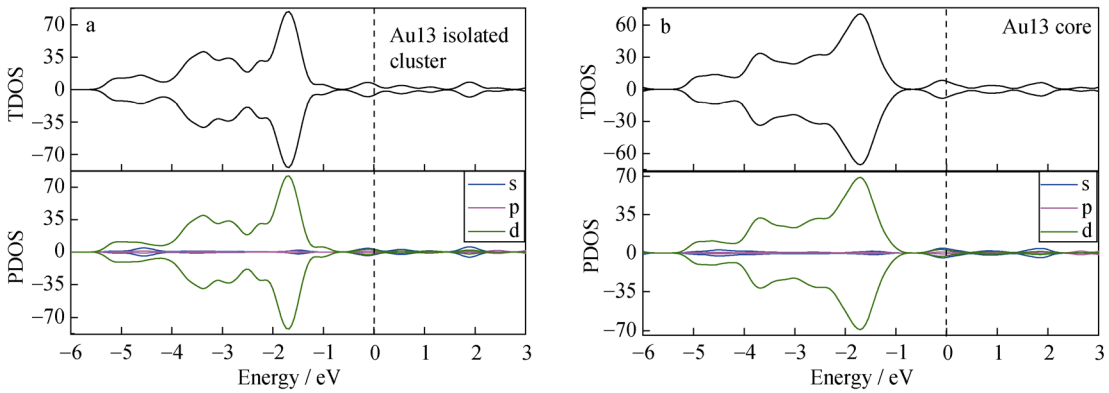

Fig. 7 Total and partial DOS of **a** Au13 isolated cluster and **b** Au13 core, where dotted lines refer to Fermi level with unit of electrons·eV^{-1}

shell. Just as DOS of $Au_{13}@ZnS_{42}$ shown in Fig. 4, when Au13 serving as inner core of ZnS outer shell, some peaks disappear compared to ZnS bulk.

3.3 Optical properties of $Au_{13}@(ZnS)_{42}$ and bulk ZnS structure

3.3.1 Absorption coefficient analysis

The optical properties of $Au_{13}@(ZnS)_{42}$ nanocluster can be systematically analyzed by means of absorption coefficient, which are presented in Fig. 8, together with ZnS bulk structure for comparison. As can be seen, for $Au_{13}@(ZnS)_{42}$ core–shell composite, there is mainly one absorption peak located in the visible-light spectrum range of about 560 nm, which is similar to the experimental detection absorption peaks occurred at 530 [17], 537 [14], and 518 nm [18]. The deviation compared with experimental result may originate from the undervalued energy gap calculated by DFT + GGA method. As shown in Fig. 8, for ZnS bulk configuration, the absorption spectrum has hardly absorption peaks in the visible-light range, suggesting that for the ZnS bulk structure, visible light is hard to be absorbed, and thus visible-light photo-catalyst gets limited. Therefrom, it can be concluded that the absorption peak of $Au_{13}@(ZnS)_{42}$ nanostructure is distinctly broadened and exhibits an obvious redshift compared to that of ZnS bulk, which suggests enhancement of visible absorption efficiency to some degree. The occurrence of redshift phenomenon may result from the strong charge transfer occurring at the interface between d-character of Au atom and p-character of surrounding S atoms. Besides, the redshift is in accord with the above discussion in DOS plots and charge density difference map.

Consequently, the visible-light absorption capability gets improved when Au cluster serving as the core of empty caged ZnS shell structure, and thus, the efficiency of photo-catalytic reaction is raised by extending the optical absorption spectra to the visible-light range.

3.3.2 Imaginary part and real part of dielectric function analysis

In addition, the frequency-dependent dielectric function was also investigated and analyzed to identify the optical properties of $Au_{13}@(ZnS)_{42}$ composite cluster. For bulk

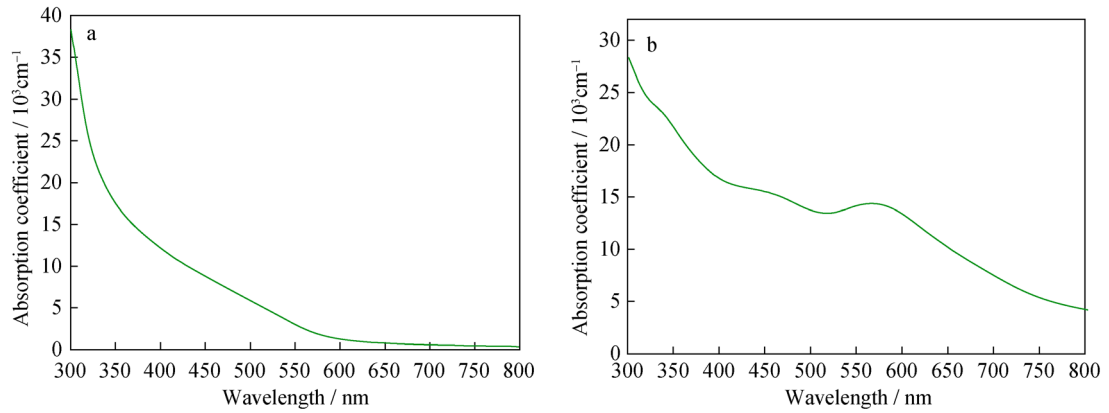

Fig. 8 Absorption coefficient of **a** ZnS bulk structure and **b** $Au_{13}@(ZnS)_{42}$ core–shell nanostructure as a function of wavelength

ZnS wurtzite-type structure, the imaginary part, $\varepsilon_2(w)$, where w denotes the frequency, (or real part, $\varepsilon_1(w)$) of the dielectric function includes two parts, the one part is $\varepsilon_2(w)_{\parallel}$(or $\varepsilon_1(w)_{\parallel}$), with the polarization vector parallel to the z direction, and the other one is $\varepsilon_2(w)_{\perp}$(or $\varepsilon_1(w)_{\perp}$) which is determined by the average of the spectra for polarizations perpendicular to z direction. Figure 9a and b presents $\varepsilon_2(w)$ and $\varepsilon_1(w)$ of dielectric function of ZnS wurtzite structure, which is consistent with the other calculated work [30]. One clearly sees that the line shape of two components for $\varepsilon_2(w)$ or $\varepsilon_1(w)$ is almost the same in the whole energy range, in order to facilitate the comparison with Au@$(ZnS)_{42}$ structure, and the averaged dielectric function with the polarization direction along the x, y and z axes, that is, $\varepsilon_2(w) = (\varepsilon_{2x} + \varepsilon_{2y} + \varepsilon_{2z})/3$ or $\varepsilon_1(w) = (\varepsilon_{1x} + \varepsilon_{1y} + \varepsilon_{1z})/3$) is also used, as shown in Fig. 9c and d.

Figure 9c and d displays the imaginary part and real part of dielectric function of Au_{13}@$(ZnS)_{42}$ and ZnS bulk material, respectively. It is known from the $\varepsilon_2(w)$ curve that the all $\varepsilon_2(w)$ peaks of Au_{13}@$(ZnS)_{42}$ weaken compared with that ZnS bulk structure in the high energy region, but there is a strong peak located in the visible-light energy region of about 2.4 eV, indicating that the Au_{13}@$(ZnS)_{42}$ nanocomposite absorbs lots of visible light. For the $\varepsilon_1(w)$ curve, the $\varepsilon_1(w)$ intensity of Au@$(ZnS)_{42}$ is also weaker than that of ZnS bulk structure, and there is also an obvious peak in the lower energy region for Au_{13}@$(ZnS)_{42}$. It is worth to note that bulk ZnS structure exhibits dielectric property in low-energy range but behaves like a metal in the high energy range of about 7–18 eV. However, the $\varepsilon_1(w)$ value of the Au@ZnS core–shell nanostructure is almost all positive and dielectric in the whole energy range. Therefore, it can be concluded that the dielectric property of Au_{13}@$(ZnS)_{42}$ nanomaterial is better than that of ZnS bulk.

4 Conclusion

In summary, although the theoretical investigation of core–shell hetero-nanostructure is quite complicated in first principle calculation, a series of optimized structures for Au_n@$(ZnS)_{42}$ core–shell nanoparticles with different n values from 6 to 16 were built. The core–shell interaction energy and second-order difference of total energy indicate a most stable structure of Au_{13}@$(ZnS)_{42}$. Furthermore, the electronic structure properties of core–shell nanostructure were studied by means of the calculated DOS and charge

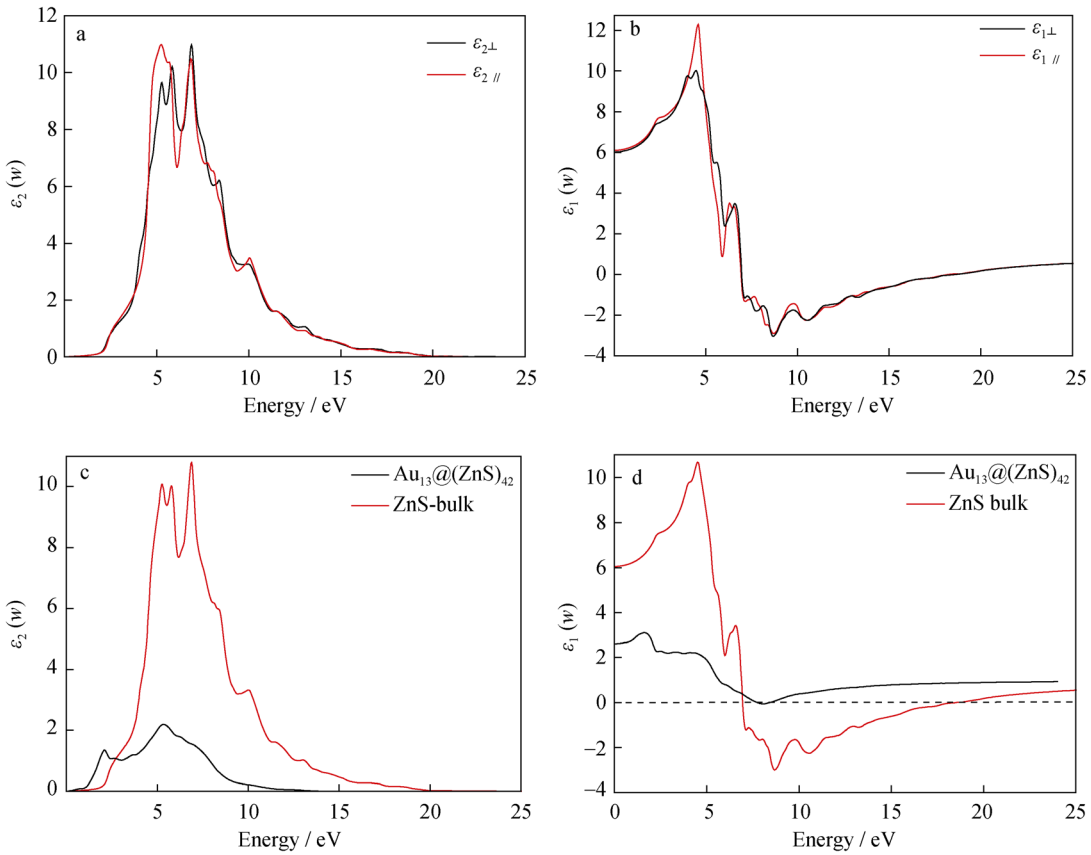

Fig. 9 Dielectric functions of **a** imaginary part and **b** real part for ZnS wurtzite structure and **c** imaginary part and **d** real part for Au_{13}@$(ZnS)_{42}$ nanostructure with ZnS bulk structure for comparison

density difference, and the results show that there are lots of electron transfers from Au atoms to ZnS shell. On the other hand, the optical properties of $Au_{13}@(ZnS)_{42}$ were also investigated based on the absorption coefficient and dielectric function; it is found that there exists a redshift of optical absorption to visible-light region from ZnS bulk to Au@ZnS core–shell structure, implying an enhancement of the photo-catalytic at visible-light region. And it is also found that the dielectric property of $Au_{13}@(ZnS)_{42}$ nanomaterial is better than that of ZnS bulk.

Acknowledgements This work was financially supported by the National Key Research and Development Program of China (Nos. 2016YFB0700500 and 2018YFB0704300).

References

[1] Gan L, Heggen M, Rudi S, Strasser P. Core–shell compositional fine structures of dealloyed Pt_xNi_{1-x} nanoparticles and their impact on oxygen reduction catalysis. Nano Lett. 2012;12(10):5423.

[2] Jackson A, Strickler A, Higgins D, Jaramillo TF. Engineering Ru@Pt core–shell catalysts for enhanced electrochemical oxygen reduction mass activity and stability. Nanomaterials. 2018;8(1):38.

[3] Li ZY, Zeng R, Jiang LJ. Pt-based core–shell catalyst for proton exchange membrane fuel cell. Chin J Rare Met. 2017;41(8):925.

[4] Wang JJ, Sun L, Mpoukouvalas K, Lienkamp K, Lieberwirth I, Fassbender B, Bonaccurso E, Brunklaus G, Muehlebach A, Beierlein T, Tilch R, Butt HJ, Wegner G. Construction of redispersible polypyrrole core–shell nanoparticles for application in polymer electronics. Adv Mater. 2009;21(10–11):1137.

[5] Lee CH, Ma Y, Jang KI, Banks A, Pan T, Feng X, Kim JS, Kang D, Raj MS, McGrane BL, Morey B, Wang X, Ghaffari R, Huang Y, Rogers JA. Soft core/shell packages for stretchable electronics. Adv Funct Mater. 2015;25(24):3698.

[6] Jovanovic AV, Flint JA, Varshney M, Morey TE, Dennis DM, Duran RS. Surface modification of silica core–shell nanocapsules: biomedical implications. Biomacromolecules. 2006;7(3):945.

[7] Atabaev T, Lee JH, Lee JJ, Han DW, Hwang YH, Kim HK, Hong NH. Mesoporous silica with fibrous morphology: a multifunctional core–shell platform for biomedical applications. Nanotechnology. 2013;24(34):345603.

[8] Park J, Kim S-W. $CuInS_2$/ZnS core/shell quantum dots by cation exchange and their blue-shifted photoluminescence. J Mater Chem. 2011;21(11):3745.

[9] Zhang N, Liu SQ, Fu XZ, Xu YJ. Synthesis of M@TiO_2 (M = Au, Pd, Pt) core–shell nanocomposites with tunable photoreactivity. J Phys Chem C. 2011;115(18):9136.

[10] Hirakawa T, Kamat PV. Charge separation and catalytic activity of Ag@TiO_2 core–shell composite clusters under UV–irradiation. J Am Chem Soc. 2005;127(11):3928.

[11] Chen ZG, Zou J, Wang DW, Yin LC, Liu G, Liu QF, Sun CH, Yao XD, Li F, Yuan XL, Sekiguchi T, Lu GQ, Cheng HM. Field emission and cathodoluminescence of ZnS hexagonal pyramids of zinc blende structured single crystals. Adv Funct Mater. 2009;19(3):484.

[12] Kim S, Kim T, Kang M, Kwak SK, Yoo TW, Park LS, Yang I, Hwang S, Lee JE, Kim SK, Kim SW. Highly luminescent InP/GaP/ZnS nanocrystals and their application to white light-emitting diodes. J. Am Chem Soc. 2012;134(8):3804.

[13] Wang XF, Xie Z, Huang HT, Liu Z, Chen D, Shen GZ. Gas sensors, thermistor and photodetector based on ZnS nanowires. J Mater Chem. 2012;22(14):6845.

[14] Misra M, Gupta RK, Paul AK, Singla M. Influence of gold core concentration on visible photocatalytic activity of gold-zinc sulfide core–shell nanoparticle. J Power Sources. 2015;294(30):580.

[15] Chen WT, Hsu YJ. L-cysteine-assisted growth of core-satellite ZnS–Au nanoassemblies with high photocatalytic efficiency. Langmuir. 2010;26(8):5918.

[16] Zhang J, Wang Y, Zhang J, Lin Z, Huang F, Yu J. Enhanced photocatalytic hydrogen production activities of Au-loaded ZnS flowers. ACS Appl Mater Interfaces. 2013;5(3):1031.

[17] Geng J. One-pot fast synthesis of spherical ZnS/Au nanocomposites and their optical properties. J Mater Sci. 2013;48(2):636.

[18] Sagheer FA, Madkour M. Au/ZnS and Ag/ZnS nanoheterostructures as regenerated nanophotocatalysts for photocatalytic degradation of organic dyes. Opt Mater Express. 2017;7(1):158.

[19] Perdew JP, Burke K, Ernzerhof M. Generalized gradient approximation made simple. Phys Rev Lett. 1996;77(18):3865.

[20] Hu YW, Huo JR, Wang XX, Wang RM. First-principles investigation on $Au_n@(ZnO)_{42}$ (n = 6–16) core–shell nanoparticles: structure stability and catalytic activity. J Phys Condens Matter. 2017;29(43):435701.

[21] Hu YW, Ji CT, Wang XX, Huo JR, Liu Q, Song YP. The structural, magnetic and optical properties of $TM_n@(ZnO)_{42}$(TM = Fe, Co and Ni) heteronanostructure. Sci Rep. 2017;7(1):16485.

[22] Shichibu Y, Suzuki K, Konishi K. Facile synthesis and optical properties of magic-number Au_{13} clusters. Nanoscale. 2012;4(14):4125.

[23] Azpiroz JM, Infante I, Lopez X, Ugalde JM, De Angelis F. A first-principles study of II–VI (II = Zn; VI = O, S, Se, Te) semiconductor nanostructures. J Mater Chem. 2012;22(40):21453.

[24] Assadollahzadeh B, Schwerdtfeger P. A systematic search for minimum structures of small gold clusters Au_n (n = 2–20) and their electronic properties. J Chem Phys. 2009;131(6):064306.

[25] Cheng HX, Wang XX, Hu YW, Song HQ, Huo JR, Li L, Qian P. Ag@ZnO Core–Shell nanoparticles study by first principle: the structural, magnetic and optical properties. J Solid State Chem. 2016;244:181.

[26] Karazhanov S, Ravindran P, Kjekshus A, Fjellvåg H, Grossner U, Svensson BG. Coulomb correlation effects in zinc monochalcogenides. J Appl Phys. 2006;100(4):043709.

[27] Cheng HX, Wang XX, Hu YW, Huo JR, Li L, Qian P, Wang RM. Theoretical investigation of geometries, stabilities, electronic and optical properties for advanced $Ag_n@(ZnO)_{42}$ (n = 6–18) hetero-nanostructure. AIP Adv. 2016;6(7):075023.

[28] Aguirre ME, Rodriguez HB, Roman ES, Feldhoff A, Grela MA. Ag@ZnO core–shell nanoparticles formed by the timely reduction of Ag^+ ions and zinc acetate hydrolysis in *N,N*-dimethylformamide: mechanism of growth and photocatalytic properties. J Phys Chem C. 2011;115(50):24967.

[29] Liu HR, Shao GX, Zhao JF, Zhang ZX, Zhang Y, Liang J, Liu XG, Jia HS, Xu BS. Worm-like Ag/ZnO core–shell heterostructural composites: fabrication, characterization, and photocatalysis. J Phys Chem C. 2012;116(30):16182.

[30] Karazhanov S, Ravindran P, Kjekshus A, Fjellvåg H, Svensson BG. Electronic structure and optical properties of ZnX (X = O, S, Se, Te): a density functional study. Phys Rev B. 2007;75(15):155104.